Supporting information for: Measuring Interfacial Polymerization Kinetics Using Microfluidic Interferometry

Arash Nowbahar,[†] Vincent Mansard,[‡] Jodi M. Mecca,[¶] Mou Paul,[§] Tina Arrowood,[§] and Todd M. Squires*,[†]

[†]*Department of Chemical Engineering, University of California Santa Barbara, CA 93106*

[‡]*Laboratory for Analysis and Architecture of Systems (LAAS-CNRS) Toulouse, 31400 Toulouse, France*

[¶]*Formulation Science, Core Research and Development, Dow Chemical Company, Midland, MI 48674*

[§]*Dow Water & Process Solutions, Dow Chemical Company, Edina, MN 55439*

E-mail: squires@engineering.ucsb.edu

Phone: (805) 893-7383

Contents

1 Microfluidic Devices

Microfluidic devices for interferometry require semi-reflective surfaces, and a channel height of $<$200μm. In addition, studying an interfacial reaction requires an interface that remains stationary throughout the duration of the measurement. For this purpose, devices consist of patterned Ag/Ti and Au-thiol regions on glass wafers bonded together with a dry film photoresist for channel walls and inlet holes. The procedure is as follows:

Inlet holes are first drilled into 4 inch Borofloat wafers (500μm thick University Wafers Inc.) which will comprise the top wall of the device. Wafers are sonicated for 3min each in acetone, isopropyl alcohol (IPA), and deionized (DI) water. Wafers are placed in a solution of NanoStrip (VWR) for 10 min, rinsed with DI water, then placed into buffered HF (MicroChemicals) for 3 min followed by another rinse.

Photolithography is performed first using the negative resist AZnLOF2035 to form a layer of thickness $\sim$ 3.5 μm. The wafers are then cleaned in oxygen plasma (Technics PEII) at 100 W power 300 mT pressure for 20 s. Layers of 5nm Ti and 50nm Au are deposited by electron beam physical vapor deposition. The wafers are left to sit in a $\sim$ 1 wt% octanethiol (Sigma) in ethanol for 48 hrs, followed by a rinse in water, and IPA. Photoresist is then lifted off by sonicating gently in acetone for $\sim$4 min. Wafers are again cleaned by sonication in acetone, IPA, and water for 3 min each.

Photolithography is repeated using mask aligner MA-6 and the positive resist AZ4110 to form a film of thickness $\sim$1.1 μm. Oxygen plasma is again used to clean the wafers at 100 W

power 300 mT pressure for 20 s. Layers of 4nm Ti and 47nm Ag and 4nm Ti are deposited by electron beam physical vapor deposition. Photoresist is then lifted off by sonicating gently in acetone for ∼4 min. Wafers are again cleaned by sonication in acetone, IPA, and water for 3 min each.

Plastic backing on dry film photoresist (KOLON Industries) is peeled and the film is lasercut into channels 3 mm wide. The width of channel was chosen to ensure channel walls are far from the drop. Dry film photoresist is pressed onto wafer on a hotplate at 120 °C. The second backing layer is subsequently peeled off. The top wafer is then aligned to the bottom wafer and pressed together. To ensure complete bonding, the device is pressed onto a hotplate at 140 °C, which slightly melts the resist. The device is cured in a UV chamber 3 mW/cm^2 for 4 min.

Tubing connectors are made from 1/16 in acrylic (McMasterCarr) that is lasercut and glued to the inlet holes using NOA 81 (Norland Products Inc.).

2 Experimental Details

m-phenylenediamine 99%, trimesoyl chloride 98%, and anhydrous decane >99% were all obtained from Sigma Aldrich. Solutions of MPD in deionized water (Milli-Q) and TMC in decane were prepared fresh for every day of experiments, to prevent oxidation or hydrolysis.

It is important that the channel height remain constant throughout the experiment. Swelling of device walls of tens of nanometers can cause the spectrum to shift, affecting the refractive index measurements. For this purpose, deionized water is first sent into the channel and left to sit for at least 15 min, allowing channel walls to soak in water.

MPD solution is then sent into the channel by hand with a syringe. Air is blown into the channel at approximately 40 mBar of pressure to create the aqueous pancake-shaped drop (see attached video). The amount of pressure the drop can withstand without getting pushed away is given by $\Delta P \sim \gamma \left(\frac{2\sin(\theta_a - 90)}{h} + \frac{1}{R} \right)$ where γ is the surface tension and θ_a is

the advancing contact angle of the aqueous drop on the hydrophobic surface. See Ref. S1, S2, and S3. It is theoretically predicted that the water drop can withstand a pressure of 17 mBar before moving.

A vessel pressurized to 40mBar is used to flow TMC with decane into the microchannel. When the oil is observed to contact the aqueous drop, the flow is stopped by exposing the inlet and outlet to the same hydrostatic pressure. The flow is typically stopped within 1-3 s (see attached video). Images are recorded for approximately 5 min. For every experiment, a new device is used.

Experiments are analyzed using a matlab algorithm to track the fringes of equal chromatic order with time.[S4] Relative shifts in wavelength are then converted to refractive index changes through the calibration curve shown in Fig.S1.

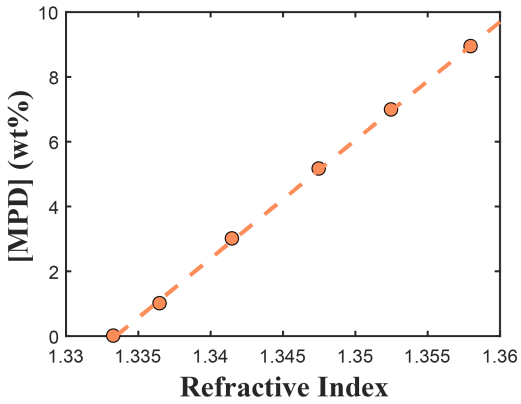

Figure S1: Calibration curve relating refractive index to MPD concentration. Dashed line shows straight line fit [MPD]=365.1050n-486.8449

3 Concentration Profiles

Concentration profiles shown in Fig. 2a reveal a depletion of MPD in the aqueous phase. To ensure this measurement is indeed due to MPD depletion, the 1D diffusion equation in cylindrical coordinates were solved using Matlab's PDE solver pdepe (Fig. S2). It is solved with a boundary condition of no flux at the center of the drop, and a concentration boundary condition at the interface determined from experimental measurements. We observe good

agreement between experimental data and the diffusion model. Here it is assumed that the flux is the same throughout the perimeter of the drop, which may be the reason for slight deviation from the experimental data.

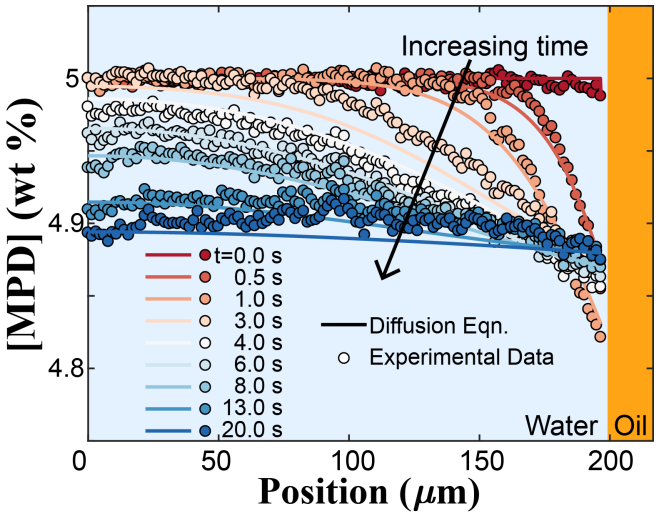

Figure S2: Concentration profiles along the drop radius (position 0 is the drop center) for the reaction between 5 wt% MPD and 0.5 wt% TMC. Lines indicate solution to diffusion equation with the measured concentration as a boundary condition at the interface.

A diffusivity, D =840μm^2/s of MPD in the aqueous phase, was used in the computation, measured through the method outlined in Ref. S4. Briefly, MPD solution is allowed to diffuse through a permeable hydrogel membrane to an open channel in a microfluidic device. The solution concentration is tracked using the same technique outlined above, and fitted to the diffusion equation to back out a diffusivity.

4 Flux Measurements

The MPD flux out of the drop is related to concentration profiles via,

$$J = -D \left.\frac{\partial [MPD]}{\partial r}\right|_{r=R} \approx -D \left.\frac{\Delta [MPD]}{\Delta r}\right|_{r=R}. \tag{1}$$

3-15 data points (4.7-23, μm depending on the noise of the data) at the edge are used to find this slope.

We estimate the smallest measurable flux to be $\sim 2 \times 10^{-5}$mol/m^{2}s ($2{\times}10^{-3}$g/m^{2}s); however, this depends on the width and noise level of the fringes, and hence changes from device to device. The flux is largest at the start of the reaction, and the most reliable; as time proceeds the fringes may 'drift' due to swelling effects.

To ensure the measured slope gives the correct measurements of the flux, we compare the flux determined this way, to the flux from a diffusion-equation solver with experimental data as a boundary condition (Fig. S3). Fluxes determined from both methods reveal good agreement, with slight deviations at long times when slopes become so gentle as to be overwhelmed by noise.

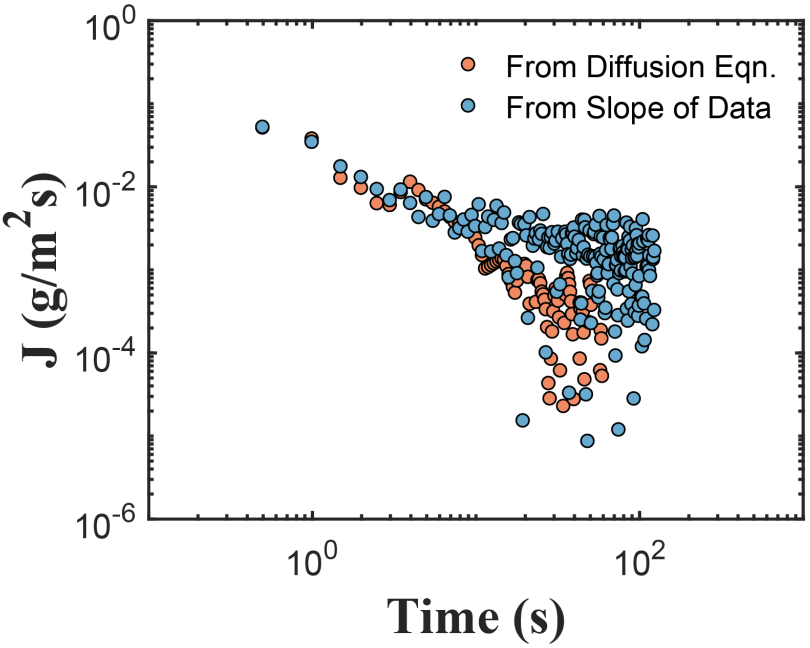

Figure S3: Red shows flux measurements by solving the diffusion equation with the interface concentration as a fixed boundary condition and taking the slope. Blue shows flux measurements by taking the slope of the experimental concentration profiles.

The fluctuations in J are estimated by calculating the ratio of the standard deviation σ (between three adjacent points) to J (Fig. S4). After approximately 10 s, the measurement fluctuates significantly ($\sigma/J > 1$). This is consistent with measurements reaching the smallest measurable flux values stated above ($2{\times}10^{-3}$g/m^{2}s).

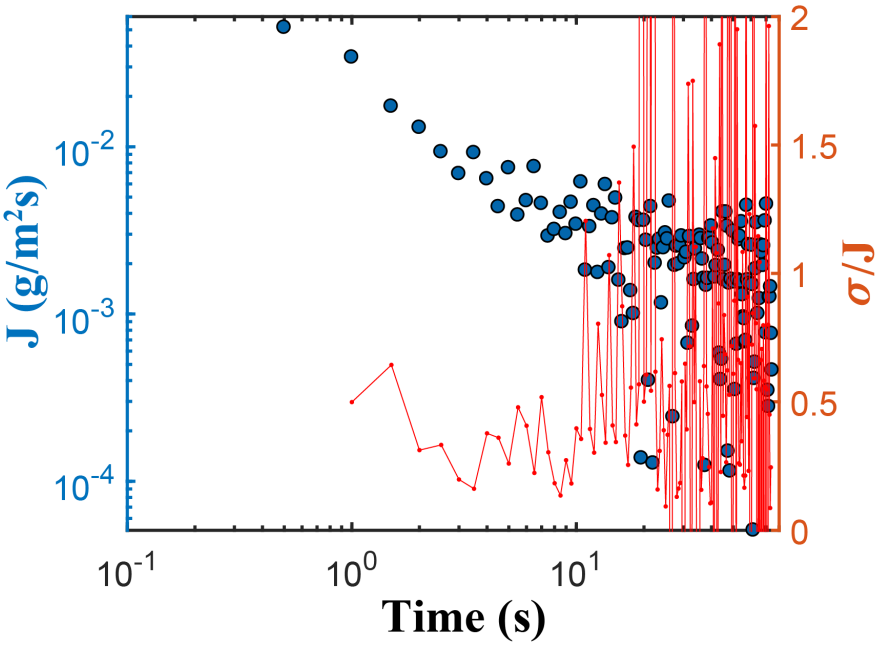

Figure S4: Blue shows flux data from Fig. 2. Red indicates the ratio of the standard deviation of every three data points, to the flux. After about 10 s, the fluctuations become larger than the the flux itself.

The amine flux out of the aqueous phase begins at some maximal value, then decays as a power-law in time with exponent between $-\frac{1}{2}$ and $-\frac{3}{2}$. Depending on the starting concentrations, we observe different behaviors in the flux. For example, at 5 wt% MPD and 0.1 wt% TMC starting concentrations, the amine flux decays as $t^{-\frac{1}{2}}$ (Fig. S5). By contrast, starting with 10 wt% MPD and 2 wt% TMC gives rise to an amine flux that decays as $t^{-\frac{3}{2}}$.

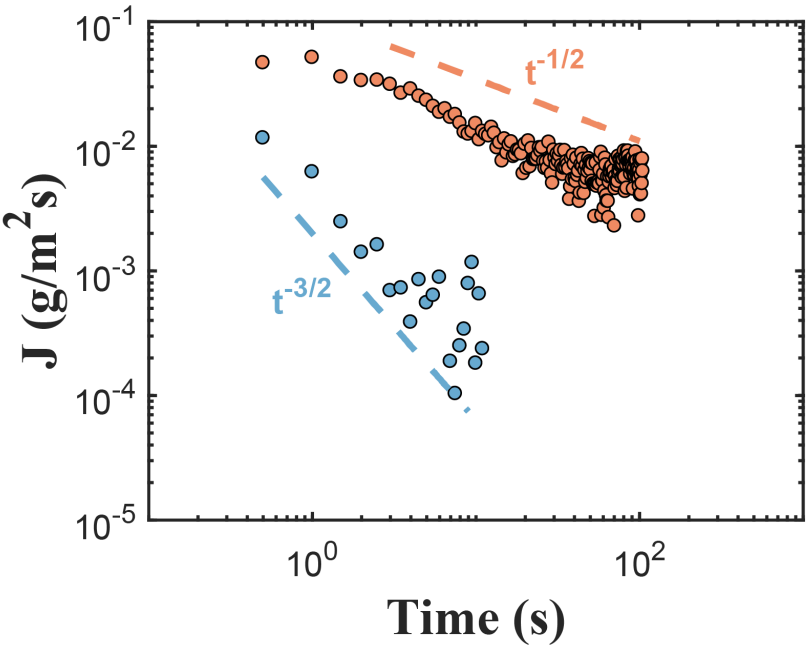

Figure S5: Amine flux out of the aqueous phase for 5 wt% MPD and 0.1 wt% TMC (red) and 10 wt% MPD and 2 wt% TMC (blue)

Integrating the flux with time yields the total mass of MPD that leaves the aqueous phase (Fig. 2). To ensure this integral is not dominated by noise, the integration is stopped when $\sigma/J > 1$ (Fig. S4).

Figure 3a shows the flux at the start of the reaction that scales linearly with starting MPD concentration. Fig. S6 shows additional measurements with fixed TMC concentrations that support this trend.

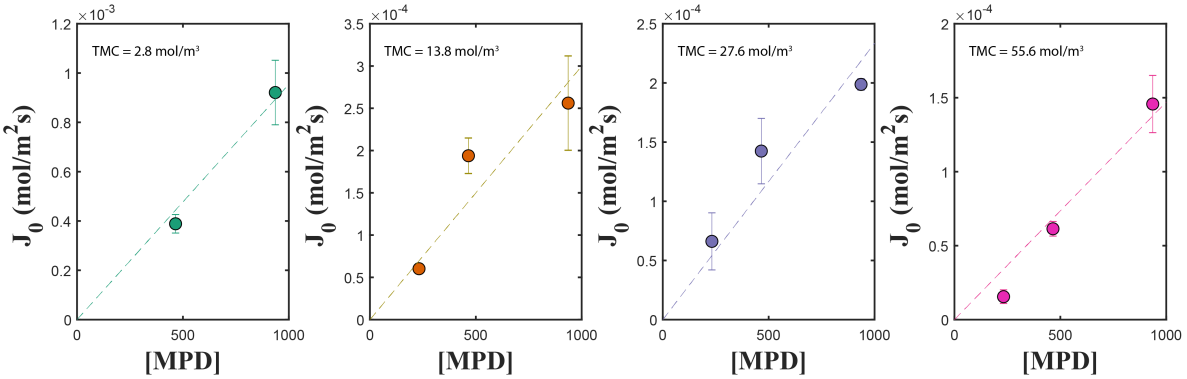

Figure S6: Flux at the start of the reaction for fixed TMC concentrations and varying MPD concentrations (in mol/m^3). Error bars indicate standard error.

5 Finite Element Computations

Finite element computations are performed using COMSOL multiphysics software to give a more detailed analysis over the scaling relations. Specifically, we solve non-dimensionalized, convection-diffusion equations with a reaction term. When oil first comes into contact with the aqueous phase, the reaction is dominated by monomer-monomer coupling reactions. We thus consider only a homogeneous, second order reaction between MPD and TMC with no phase separation. Moreover, we restrict the study to quasi-steady equations,because the reaction-diffusion boundary layer develops much quicker than concentration changes occur in the aqueous drop. The water drop is considered to simply be a solid surface with a slip boundary condition, and a concentration boundary condition of $K[MPD]_0$, where K is the oil-water partition coefficient and $[MPD]_0$ is the starting MPD concentration in solution. The concentration of MPD, $[MPD]$, and TMC, $[TMC]$, are non-dimensionalized by $K[MPD]_0$, and the starting TMC concentration $[TMC]_0$ respectively, giving the dimensionless concentrations $[\widetilde{MPD}]$, and $[\widetilde{TMC}]$. The flow equations are solved under a thin channel limit (Hele-Shaw approximation), given that the channel height is 25 μm compared to a drop radius of 250 μm:

$$-\widetilde{\nabla}\widetilde{P} + \widetilde{\nabla}^2\widetilde{\boldsymbol{u}}_{oil} - \frac{12\widetilde{\boldsymbol{u}}_{oil}}{\widetilde{d}^2} = 0, \tag{2}$$

where $\widetilde{u}_{oil}$ is the oil flow non-dimensionalized by the characteristic flow velocity U_0, $\widetilde{P}$ is the non-dimensionalized pressure, d is the non-dimensional channel height. All length-scales are non-dimensionalized by the drop radius R. Conservation of mass for MPD and TMC are given by:

$$\widetilde{\nabla}^2[\widetilde{MPD}] - Pe\widetilde{\boldsymbol{u}}_{oil} \cdot \widetilde{\nabla}[\widetilde{MPD}] - 6Da[\widetilde{MPD}][\widetilde{TMC}] = 0, \tag{3}$$

$$r_D\widetilde{\nabla}^2[\widetilde{TMC}] - Pe\widetilde{\boldsymbol{u}}_{oil} \cdot \widetilde{\nabla}[\widetilde{TMC}] - 6Da[\widetilde{MPD}][\widetilde{TMC}]r = 0 \tag{4}$$

where the dimensionless groups emerge:

$$Pe = \frac{U_0 R}{D_{MPD}},\ Da = \frac{k[TMC]_0 R^2}{D_{MPD}},\ r = \frac{K[MPD]_0}{[TMC]_0},\ r_D = \frac{D_{TMC}}{D_{MPD}}$$

where D_{MPD} and D_{TMC} are the diffusivities of MPD and TMC, respectively, in the oil phase. Figure S7 shows the results of simulations for a particular set of parameters. Fig S7a shows the concentration profiles of $[\widetilde{MPD}]$ at the leading edge of the drop, where the flow is in the $\widetilde{y}$ direction. For increasing Da, the thickness of the boundary layer δ decreases. In fact, δ scales as $Da^{-1/2}$. This can be seen by looking at Da=39 and 158 and observing the concentration profile decrease by half in the presence of a four-fold increase in Da. Fig S7b shows spatial $[\widetilde{MPD}]$ profile throughout the drop. The reaction-diffusion boundary layer is slightly thicker in the back. More noticeably, $[\widetilde{TMC}]$ at the back of the drop (downstream in the flow direction) is more depleted, and the concentration field is asymmetric. This is due to the nature of the flow, replenishing TMC at the front of the drop more than at the back.

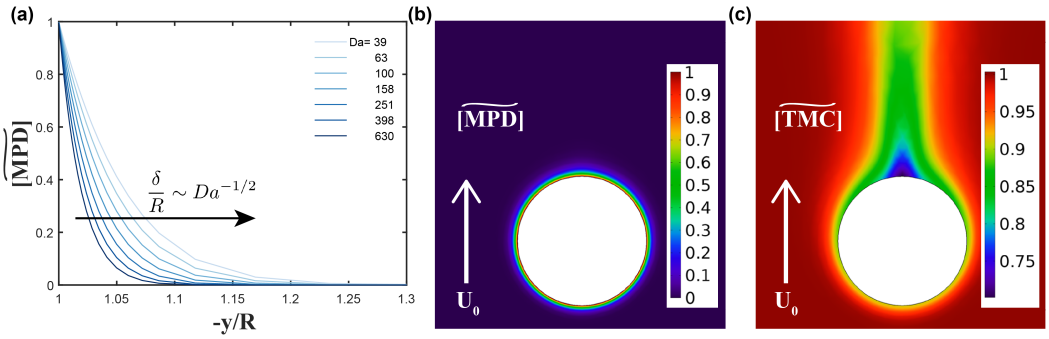

Figure S7: (a) $[\widetilde{MPD}]$ from finite element simulations from the leading edge of the drop with Pe=50, r_D=1, and $r = 0.05$, with varying Da. (b-c) 2D colormap showing the reaction diffusion boundary layer around the drop with arrow indicting direction of flow. Simulation for Pe=50, r_D=1, and $r = 0.05$, and Da=63. (c) $[\widetilde{TMC}]$ is depleted near the back of the drop, showing an asymmetric reaction diffusion boundary layer.

If the effect of the reaction is weak compared to the strength of convection ($6Da < Pe$), convection dominates the flux of MPD out of the drop. For our experiments we estimate $Pe \sim 125$. The flow could be slower than this, however, due to water droplets in the tubing

(formed during the creation of the pinned drop), creating extra resistance, or because oil/air contact lines randomly pin as the flow enters the channel. The dimensionless flux, $\widetilde{J}$ is shown in Fig. S8a for varying Da. At higher Da, the flux is dominated by a reaction diffusion boundary layer given by the scaling $\widetilde{J} \sim (6Da^{1/2})$. Dimensionally, this is given as: $J \sim K[MPD]_0\sqrt{6k[TMC]_0 D_o}$. We can find the deviation of simulations from this scaling by plotting $\widetilde{J}/(6Da^{1/2})$ (Fig. S8b). This deviation ranges from ~ 0.7 to ~ 1.4 over a few decades in Da. For our purposes, we take the proportionality constant to be 1 ± 0.2.

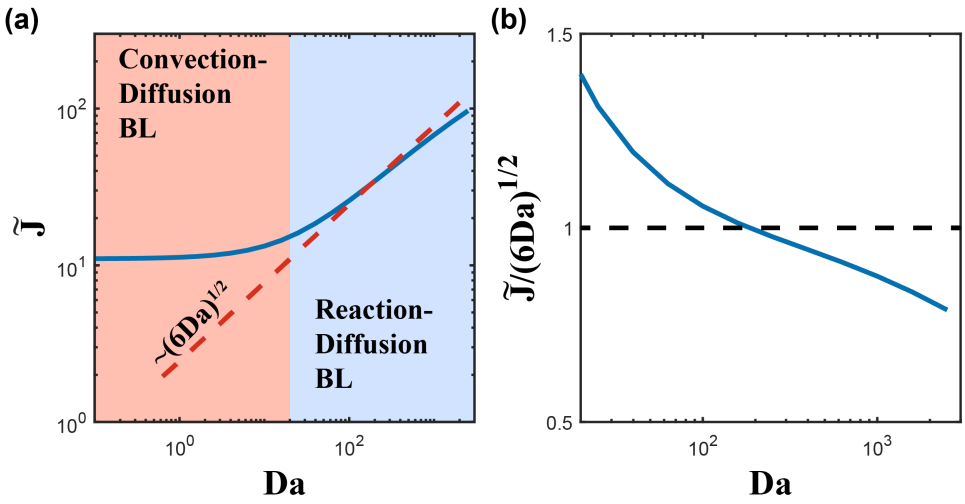

Figure S8: (a) Dimensionless flux at the leading edge of the drop, upstream to the flow for various Da, for $Pe = 125$, $r_D = 1$, and $r = 0.05$. When the releative strength of the reaction is low, convective transport dominates the flux of amine. When the relative strength of the reaction is large, the reaction dominates the flux of amine. (b) Deviation of flux from predicted scaling.

6 MPD Partition Coefficient

The oil/water partition coefficient K was measured using a similar method to Ref. S5. One milliliter of aqueous MPD solutions are placed with one milliliter of decane, shaken, and stirred at 1000 rpm for 5 hrs to allow equilibration. Equilibration is insured by comparing solution concentrations at various times, and by different mixing methods (e.g. sonicating to form droplets that equilibrate faster), revealing little differences in measured concentrations. UV absorbance of oil samples at 297 nm are subsequently measured with a Tecan M220

Infinite Pro plate reader. This absorbance is then converted to concentration by measuring the absorbances of known concentrations: a solution of 10 mg/mL MPD in isopropyl alcohol is made, then dispersed into decane solutions (Fig. S9). The isopropyl alcohol is shown to not affect the absorbance spectrum as indicated in Fig. S9a.

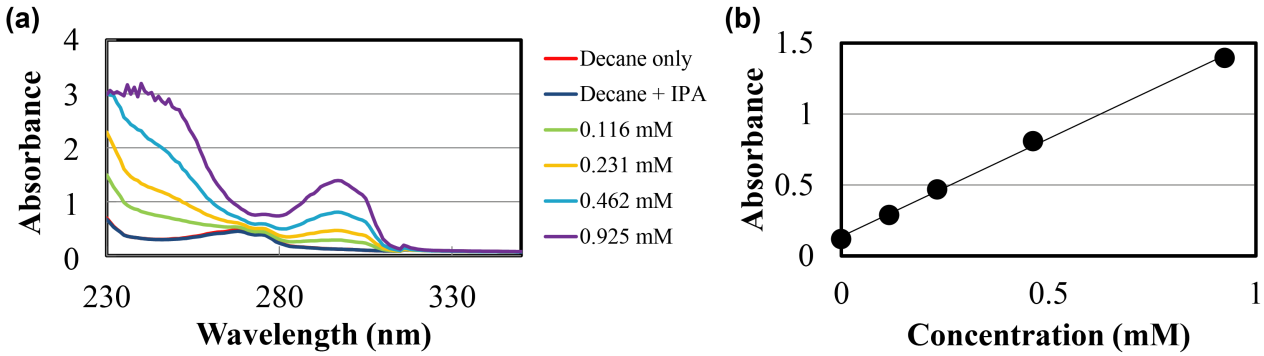

Figure S9: (a) Absorbance spectrum for various MPD concentrations in decane. (b) Absorbance at 297 nm for various MPD concentration in decane.

Figure S10 shows MPD concentrations in the oil versus the water after equilibration. Five samples are measured at each aqueous concentration. The slope indicates a partition coefficient of $K = 0.0022 \pm 5 \times 10^{-5}$. Using an alternative technique (not reported here), we measure $K = 0.0026 \pm 2.5 \times 10^{-4}$. Taking a conservative value we use $K = 0.0024 \pm 2 \times 10^{-4}$. This value is similar to that reported elsewhere for heptane/water.[S6]

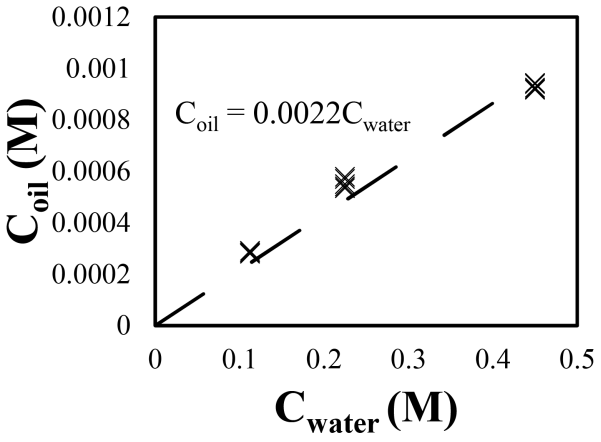

Figure S10: MPD concentrations in the oil vs the water after equilibration. Five samples are measured at each concentration. Slope indicates the oil/water partition coefficient.

7 MPD Diffusivity in Oil Phase

The diffusivity of MPD in decane was obtained using pulsed field gradient nuclear magnetic resonance (PFG NMR). Experiments were performed at 20 °C on a 300MHz Bruker SWB Spectrometer, using a stimulated echo pulse sequence. To obtain the best possible signal to noise ratio, $C_{10}D_{22}$ decane (99 atom% Sigma Aldrich) was saturated with MPD. Residual internal $C_{10}D_{21}H$ (chemical shift 1.26) was used as a standard. The diffusion coefficient was obtained by fitting the decay in the echo signal to the Stejskal-Tanner equation,

$$I = I_0 \exp(-D(\gamma\delta G)^2(\Delta - \delta/3)) \tag{5}$$

where D is the self-diffusivity, I is the signal intensity, I_0 the intensity signal at zero gradient, $\gamma = 4258$ Hz/G the gyromagnetic ratio, δ the pulse duration (set to 1.01 ms), and Δ is the diffusion time (set to 20 ms). The applied linear gradient was varied from 0-127 G/cm, with the number of acquisitions for each experiment of 64. Magnetic field gradients were calibrated using a 50/50 mixture of HDO and D_2O.

MPD contains 4 distinct protons, with measured chemical shifts of 6.75, 5.92, 5.79, and 3.19 ppm (Fig. S11a). Each of these protons is well resolved, thus each can be analyzed independently by fitting each to eqn. (5) to find self-diffusivities. Figure S11b shows the decaying intensity with gradient strength for the proton at 5.79 ppm. We define the diffusivity of the MPD molecule as the mean value obtained from the distinct proton resonances. This gives an MPD diffusivity of $D_o = 1630 \pm 90$ $\mu m^2/s$.

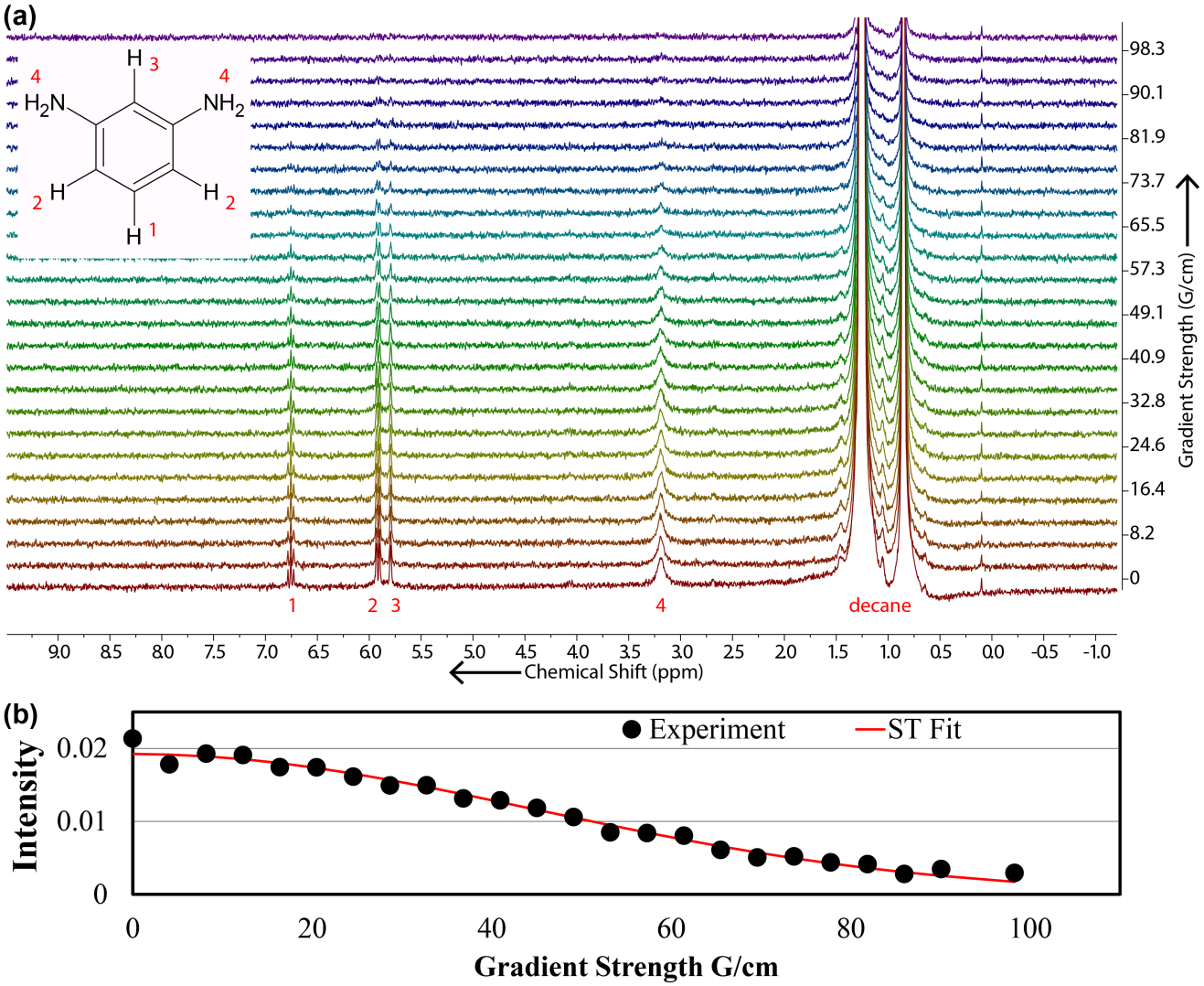

Figure S11: (a) ^{1}H PFG NMR spectra with varying gradient strength. Peaks corresponding to MPD protons are indicated with numbers. Here the signal from residual $C_{10}D_{21}H$ shows up as a large peak. (b) Intensity with increasing gradient strength for proton at 5.79ppm, showing the fit to the Stejskal-Tanner equation.

References

(S1) Zhao, B.; Moore, J. S.; Beebe, D. J. *Analytical Chemistry* **2002**, *74*, 4259–4268.

(S2) Zhao, B.; Moore, J. S.; Beebe, D. J. *Science* **2001**, *291*, 1023–1026.

(S3) Zhao, B.; Viernes, N. O.; Moore, J. S.; Beebe, D. J. *Journal of the American Chemical Society* **2002**, *124*, 5284–5285.

(S4) Vogus, D. R.; Mansard, V.; Rapp, M. V.; Squires, T. M. *Lab Chip* **2015**, *15*, 1689–1696.

(S5) Behera, S.; Suresh, A. K. *Polymer (United Kingdom)* **2017**, *127*, 28–44.

(S6) Leo, A.; Hansch, C.; Elkins, D. *Chemical Reviews* **1971**, *71*, 525.